S.M.K. Chaitanya* and P. Rajesh Kumar

Oppositional Gravitational Search Algorithm and Artificial Neural Network-based Classification of Kidney Images

https://doi.org/10.1515/jisys-2017-0458 Received July 14, 2017; previously published online April 13, 2018.

Abstract: Ultrasound (US) imaging has been broadly utilized as part of kidney diagnosis because of its ability to show structural abnormalities like cysts, stones, and infections as well as information about kidney function. The main aim of this research is to effectively classify normal and abnormal kidney images through US based on the selection of relevant features. In this study, abnormal kidney images were classified through gray-scale conversion, region-of-interest generation, multi-scale wavelet-based Gabor feature extraction, probabilistic principal component analysis-based feature selection and adaptive artificial neural network technique. The anticipated method is executed in the working platform of MATLAB, and the results were analyzed and contrasted. Results show that the proposed approach had 94% accuracy and 100% specificity. In addition, its false-acceptance rate is 0%, whereas that of existing methods is not <27%. This shows the precise prediction level of the proposed approach, compared with that of existing methods.

Keywords: Probabilistic principal component analysis (PPCA), oppositional gravitational search algorithm (OGSA), artificial neural network (ANN), k-nearest neighbors (KNN), genetic algorithm-based ANN (GA-ANN).

1 Introduction

In medical imaging, any error can cause a threat to proper diagnosis; hence, accurate identification of medical image is a difficult task. To ensure the statistical significance of studies, sufficient amount of data from clinical trials and medical examinations has to be collected. Collection of clinical analyses and laboratory results from electronic databases is useful for research, medical investigations, epidemiological studies, quality control and so on [4, 12]. Many different imaging technologies and implications are covered by medical imaging, such as X-ray-based methods like radiography and computed tomography (CT), magnetic resonance imaging (MRI), ultrasound (US), nuclear medicine with positron emission tomography (PET), single photon emission computed tomography (SPECT) and other methods in optical imaging. To solve complex geometric problems arising in medical image processing, the classification method of segmentation, shape extraction, three-dimensional (3D) modeling and registration of medical data efficient algorithms are required.

The reconstruction of 3D shapes (of organs, bones, tumors, etc.) from two-dimensional (2D) slice is derived from MR or CT scans, which is a key problem in medical computation. A proper surface connects a set of contour data points [12, 16, 17], which are determined by the typical geometric problem. Medical image segmentation is the basis of medical image analysis and understanding. It plays an important role in pathology analysis and treatment and clinical diagnosis. In the imaging process, the formation of medical image is susceptible to some factors such as noise and effect of bias field. These factors lead to intense homogeneity

^{*}Corresponding author: S.M.K. Chaitanya, ECE Department, G.V.P. College of Engineering (Autonomous), Visakhapatnam, Andhra Pradesh 530048, India, e-mail: smkchaitanya0417@gmail.com

P. Rajesh Kumar: Department of Electronics and Communication Engineering, Andhra University College of Engineering (Autonomous), Visakhapatnam, Andhra Pradesh 530003, India

in the image. For image segmentation, numerous software tools are available, both commercial and open source. In image segmentation, the disadvantage of open-source software is that they do not support parallelimage processing. Large-scale processing leads to long computational times and high computational power requirements.

The method consists of automatic multi-resolution image parameterization, which is based on texture description with specialized association rules coupled with image evaluation and machine learning methods. Since this approach yields a large number of relatively low-level features (although much more informative than simple pixel intensity values), we have used additional dimensionality reduction techniques either by discarding some features (feature selection) or by combining them into more informative, high-level features (feature construction) [7, 13, 14, 19].

2 Literature Survey

Huang et al. [9] have explained the segmentation of US kidney images. Using trained prior shapes, they employ a parametric super-ellipse as a global prior shape for a human kidney. The Fisher-Tippett distribution was employed to describe the gray-level statistics. By combining the gray-level statistics with a global character of a kidney shape, they used an active contour model to segment the US kidney images. It involves two sub-problems: one was the optimization of the parameters of a super-ellipse and the other was the segmentation of a US kidney image. An alternating minimization scheme was used to simultaneously optimize the parameters of a super-ellipse and segment an image.

Gunasundari et al. [5] have explained the computer-aided diagnostic system, which plays an important role in the detection of cancer. Feature selection was an important preprocessing step in the classification phase of the diagnostic system. The feature selection was an NP-hard challenging problem that provides many applications in the area relevant to expert and intelligent system. Two modified Boolean particle swarm optimization algorithms, namely velocity bounded and improved velocity bounded, were used to solve the feature selection problem.

Odeh et al. [11] have proposed the use of early imaging markers to predict future renal deterioration in infants with posterior urethral valves. Using National Institutes of Health-sponsored image-processing software, they analyzed a series of initial postnatal US images of the serial posterior urethral valve of the cases seen at a single tertiary referral center. Echogenicity and corticomedullary differentiation were objectively measured as the ratios relative to the adjacent liver or spleen and also between the cortex and the medulla. At last follow-up, the primary study outcome and renal function were dichotomized based on glomerular filtration rate and/or need for renal replacement therapy. Estimates of renal parenchyma quantity and quality measured on initial postnatal US carry prognostic value by determining future risk of stage 5 chronic kidney disease in patients with posterior urethral valves.

Subramanya et al. [15] have explained a computer-aided classification system for three kidney classes, viz. normal, medical renal disease (MRD) and cyst using B-mode US images. Thirty-five B-mode kidney US images consisting of 11 normal, eight MRD and 16 cyst images have been used. Regions of interest (ROIs) have been marked by the radiologist from the parenchyma region of the kidney in case of normal and MRD cases and from regions inside the lesions for cyst cases. To evaluate the contribution of texture features extracted from de-speckled images for the classification task, original images have been preprocessed by eight de-speckling methods. Six categories of texture features were extracted. A one-against-one multi-class support vector machine classifier has been used, which was based on overall classification accuracy (OCA), and features from the ROIs of original images were concatenated with the features from the ROIs of preprocessed images. Based on OCA, few feature sets were considered for feature selection.

Di Noia et al. [3] have studied IgA nephropathy, a disease of the kidneys that affect millions of people worldwide and leads to end-stage kidney disease (ESKD), which requires renal replacement therapy through dialysis or kidney transplantation. Tools are needed to help clinicians predict ESKD risk in IgAN patients, and

this was highly recognized in the medical field as a software tool that exploits the power of artificial neural networks (ANNs) to classify patients' health status potentially leading to ESKD. In a period of 38 years at the University of Bari, the classifier leverages an ensemble of networks trained using collected data. The developed tool has been made available both as an online Web application and as an Android mobile app.

Gupta and Karmeshu [6] raised a major issue in the characterization of clinical US B-mode images and it has been used to identify a few probability distributions that could broadly classify images of human organs. By resorting to the statistical characterization of gray levels in 100 clinical B-mode US kidney images, the concern is addressed. A detailed investigation of central and peripheral kidney regions was carried out. The Pearson family of distributions was employed as a means to model the images and to provide analytical expression of the suitable pdf in terms of parameter κ. In most cases, type I Pearson distribution (corresponding to negative κ) yields the best fit.

3 Problem Definition

In recent years, great progress has been made in automated systems for detecting kidney diseases through ultrasonic systems, which allow the extraction of greater amount and quality of information during imaging of patients. The use of feature extraction, image analysis and pattern recognition techniques for classification are most suited for the evaluation of global conditions. However, no technique has been proven to be best or has improved the accuracy of the system. Hence, improving the classification accuracy by improving the existing classification system as well as the preprocessing models is necessary. The lack of solution and the above-mentioned problems motivated this research.

4 Proposed Normal/Abnormal Kidney US Image Classification **Technique**

4.1 Contribution of the Proposed Research

US is the most favored therapeutic methodology in analyzing delicate tissue, for example, brain and kidneys. In contrast with other imaging methods such as PET and MRI, US is non-invasive and does not expose the patient to radiation, has low cost, requires minimal scan time and its operation is adaptable. Hence, great improvement is needed on delivering better and innovative US in terms of portability, cost, and size. When using US for diagnosis, procedure, problem-specific visual cues or features must be considered, in keeping in mind the goal of sorting a tissue image as one of the feasible classifications. These features originate from the discernible attributes of cells or nuclei, for instance, size, shape or texture. However, no strategy turned out to be ideal or has enhanced the exactness of the framework.

Hence, in this article, a computer-aided system is introduced for the classification of normal and an abnormal US kidney image, which is based on novel feature extraction and classification methods, to improve the accuracy of classification results. The proposed novel feature extraction method includes a set of multi-scale wavelet-based features and the suggested classification method like ANN approach, where the weight parameters are chosen optimally through opposition-based GSO algorithm (OGSA). First, the multiscale wavelet-based features were extracted from the ROI of each image, and the probabilistic principal component analysis (PPCA) is performed to reduce the number of features. The selected features were utilized in the design and training of the proposed adaptive neural network (adaptive ANN) classifier. The ANN will classify the images as normal or abnormal through the extracted features. Here, the ANN is hybridized with oppositional-based gravitational search algorithm (OGSA) for better classification. The block diagram of the proposed adaptive ANN abnormality classification method is given in Figure 1.

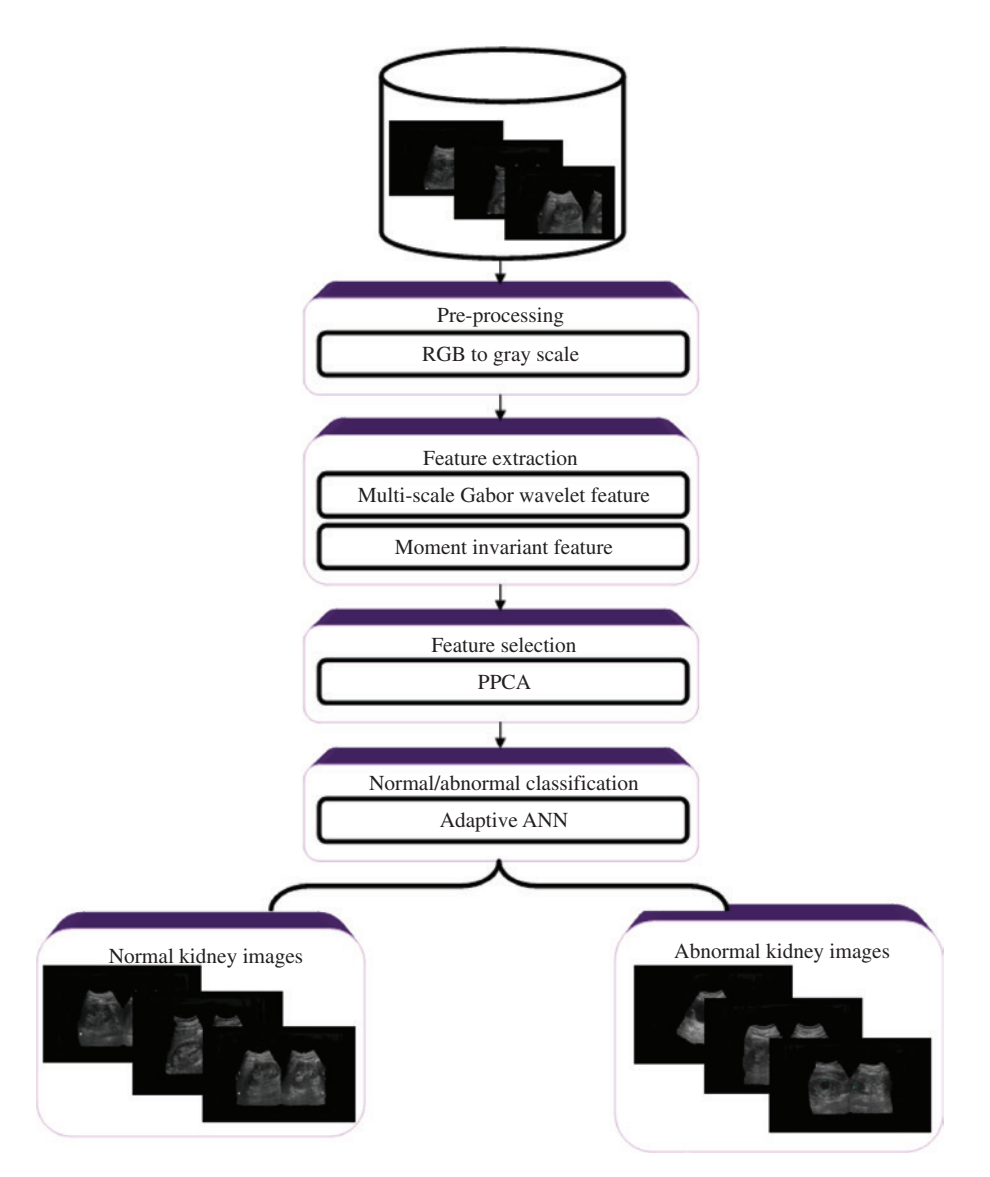


Figure 1: Proposed Kidney Image Classification Model.

4.2 Sketch of the Proposed Procedure

The steps involved in the proposed method are

- Preprocessing
- 2. Gabor wavelet-based feature extraction
- Feature selection by PPCA 3.
- Normal/abnormal classification by adaptive ANN

Each stage of the proposed normal/abnormal classification method is detailed in the upcoming section.

4.2.1 Preprocessing

Preprocessing is the fundamental step of image processing techniques. Preprocessing procedures are usually done to remove the unwanted noise components of the image. Here, color-to-gray conversion is performed to reduce the processing complexity. Finally, ROI generation is performed to reduce the interference of irrelevant regions.

4.2.2 Gabor Wavelet-based Feature Extraction

To define a class, the uniqueness of kidney image is represented by selecting the features. In this approach, five-level wavelet decomposition is made. At each level, the mean, covariance and seven moment invariant features are extracted. Further, for the decomposed horizontal and vertical details, the Gabor features are extracted four different wavelength and six different orientations.

5-Level wavelet decomposition: The 2D discrete wavelet transform (2D-DWT) is used to represent an image for multi-resolution analysis. The 2D-DWT performs a sub-band coding of an image in terms of spectral spatial/frequency components using an iterative and recursive process. The image is first represented by LH (horizontal), HL (vertical) and HH (diagonal) sub-bands that encode the image details in three directions and an LL sub-band that provides an approximation of it. The LL sub-band is considered for further decomposition levels.

Assume p(m, n) as a given image of size $(M \times N)$. At each scale s with (s > 0), the wavelet transform decomposes into four wavelet bands. From the frequency details, the horizontal and vertical wavelet bands $(D_{-}^{H}p, D_{-}^{H}p)$ at scale s are extracted. For the horizontal and vertical coefficients, the mean, variance and seven moment invariant features were extracted for five different scales.

Thus, as a result 90 [i.e. $5*2(H, V)*(mean+variance+(\psi_1+\psi_2...\psi_n))$] features were extracted. The extracted features were

Mean: This is the average value:

mean =
$$\left(\frac{1}{ZW}\right)\sum_{z=1}^{Z}\sum_{w=1}^{W}F(z, w),$$
 (1)

where F(z, w) represents the horizontal/vertical wavelet sequence.

Variance: This is defined as the sum of the square distance of each term in the mean distribution divided by the number of terms in the distribution:

variance=
$$\frac{1}{(Z-1)(W-1)} \sum_{z=1}^{Z} \sum_{w=1}^{W} (F(z, w) - \text{mean})^{2}$$
. (2)

Moment invariant features: These were introduced by Hu [8], based on the normalized central moments. The 2D (s, t)th-order moment is defined as

$$M_{st} = \int_{-\infty}^{\infty} \int_{-\infty}^{\infty} z^s w^t F(z, w) dz dw,$$
 (3)

where s, t = 0, 1, 2, ...

Moreover, the 2D (s, t)th-order central moment from which the invariant features are attained is defined as

$$CM_{st} = \vartheta_{st} = \int_{-\infty}^{\infty} \int_{-\infty}^{\infty} (z - \overline{z})^{s} (w - \overline{w})^{t} F(z, w) dz dw, \tag{4}$$

where (\bar{z}, \bar{w}) is the image centroid pixel point.

The image centroids are computed as

$$\bar{z} = \frac{M_{10}}{M_{00}}; \bar{w} = \frac{M_{01}}{M_{00}}.$$
 (5)

It is seen that Equations (3) and (4) are equivalent to each other when the center of moment, M_{st} , is equal to the image centroids.

The scale invariance is attained by normalization, and the normalized central moments can be defined as

Normalized
$$CM_{st} = \lambda_{st} = \frac{\vartheta_{st}}{\vartheta_{st}^{\varepsilon}}; \varepsilon = \frac{(s+t+2)}{2},$$
 (6)

where s+t=2, 3, 4, ...

The moment invariant features are

$$\psi_1 = \lambda_{20} + \lambda_{02} \tag{7}$$

$$\psi_2 = (\lambda_{20} + \lambda_{02})^2 + 4\lambda^2 \tag{8}$$

$$\psi_{3} = (\lambda_{30} - 3\lambda_{12})^{2} + (3\lambda_{21} - \lambda_{03})^{2} \tag{9}$$

$$\psi_{4} = (\lambda_{30} + \lambda_{12})^{2} + (\lambda_{21} + \lambda_{03})^{2} \tag{10}$$

$$\psi_{5} = (\lambda_{30} - 3\lambda_{12})(\lambda_{30} + \lambda_{12}) \left[(\lambda_{30} + \lambda_{12})^{2} - 3(\lambda_{21} + \lambda_{03})^{2} \right] + (3\lambda_{21} - \lambda_{03})(\lambda_{21} + \lambda_{03}) \left[(3\lambda_{30} + \lambda_{12})^{2} - (\lambda_{21} + \lambda_{03})^{2} \right]$$
(11)

$$\psi_6 = (\lambda_{20} - \lambda_{02}) \left[(\lambda_{30} + \lambda_{12})^2 - (\lambda_{21} + \lambda_{03})^2 \right] + 4\lambda_{11}(\lambda_{30} + \lambda_{12})(\lambda_{21} + \lambda_{03})$$
(12)

$$\psi_{7} = (3\lambda_{21} - \lambda_{03})(\lambda_{30} + \lambda_{12}) \left| (\lambda_{30} + \lambda_{12})^{2} - 3(\lambda_{21} + \lambda_{03})^{2} \right| - (\lambda_{30} - 3\lambda_{12})(\lambda_{21} + \lambda_{03})[3(\lambda_{30} + \lambda_{12})^{2} - (\lambda_{21} + \lambda_{03})^{2}]$$
(13)

The seven moment invariant features are extracted for the horizontal and vertical coefficients obtained from the wavelet decomposition.

4. Gabor feature: Gabor filters are applied to an image to extract features from many scales or frequencies which are aligned at different angles. Here, the Gabor features are computed for the wavelet decomposed image. A Gabor filter can be represented by

$$g(z, w, \gamma, \omega) = \frac{1}{2\Pi\sigma_z\sigma_w} e^{\frac{-1}{2}\left(\frac{z_1^2}{\sigma_z^2} + \frac{w_1^2}{\sigma_w^2}\right)},$$
(14)

where σ_z and σ_w are the standard deviations in z, w directions; $\gamma=1/\text{central}$ frequency represents the wavelength and ω represents the orientation angle. The frequency and orientation gives major detail about the shape and patterns of the kidney image. Here, the features were extracted for four different wavelengths (i.e. $\gamma=\{2,4,6,8\}$) and six different orientations (i.e. $\omega=\{0,30,60,90,120,150\}$). Moreover, parameters z_1 and w_1 can be summarized as

$$z_1 = z\cos\omega + w\sin\omega \tag{15}$$

$$W_1 = -z\cos\omega + w\sin\omega \tag{16}$$

From the Gabor filter, $g(z, w, \gamma, \omega)$, the Gabor features can be extracted as

$$F(g) = F(z, w) * g(z, w, \gamma, \omega). \tag{17}$$

Here, the Gabor features are computed for the wavelet decomposed image with four different central frequencies and six orientations and yields 24 features at each level of decomposition. As five-level wavelet decomposition is performed, 2160 features [i.e. (5*2*(7+2))*4*6=90*24=2160] were attained for each image.

Thus, the normal/abnormal classification of kidney images based on the extracted 2160 features is a tedious process. Hence, PPCA-based feature selection is introduced.

4.2.3 Feature Selection by PPCA

For better classification the selection of correct number of feature subset is a challenging task. An incorrect choice may lead to over-extraction or under-extraction.

PCA has some limitations. The main limitations are:

- A lack of a probabilistic or generative model.
- The technique is globally linear.
- The covariance matrix is difficult to be evaluated in an accurate manner.

To overcome these two limitations Tipping and Bishop [18] propose a mixture model for probabilistic PCA. PPCA, which allows us to reconstruct the optimal shape, is an efficient tool to reduce the dimension of a data set consisting of a large number of interrelated variables while retaining most of the variations. PPCA extracts projection vectors which contribute to highest covariance and these projection vectors are used to reduce feature dimension. It is achieved by transforming the data set to a new set of ordered variables according to their variances or their importance. Also, PPCA provides a way to compute the low-dimensional representation with a well-formed probability distribution of higher-dimensional data.

In this research, the probabilistic PCA selects K-eigenvectors corresponding to K-highest eigen values from the feature input, i.e. one-dimensional principal components, that maximize the likelihood of the data. Thus, as a result, only 10 features were selected from the 2160 features.

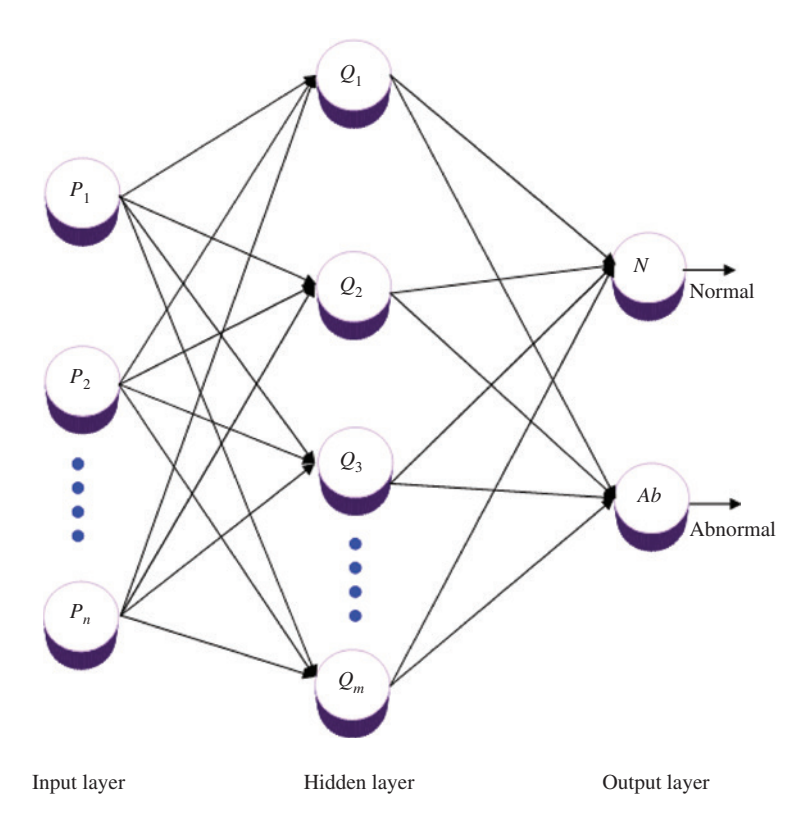


Figure 2: Artificial Neural Network Structure.

4.2.4 Normal/Abnormal Classification by Adaptive ANN

AANs are inspired by the structure and human brain functionality, which can be imagined as a network consisting of densely interconnected processing elements called neurons. The neural network encompasses a sequence of nodes (neurons) that contain numerous associations among further nodes. The aim is to produce a useful model applicable for problem solving and knowledge engineering. The structure of ANN is given in Figure 2.

The ANN architecture consists of three layers: an input layer, an output layer and one or more hidden layers between these two layers. There are two very significant segments in the neural network system: training phase and testing phase. In the training phase of ANN, the network is trained with the known classes based on the search of minimum error (difference between ANN output and target) as a function of the ANN weights and biases. The interconnection weights are randomly assigned and updated until the error gets minimized.

The projected procedure employs the adaptive ANN for the categorization of normal/abnormal kidney images. At this time, the conventional neural networks are customized by means of OGSA, which is engaged in the optimization of the weight in the neural network. The anticipated adaptive ANN utilizes one input layer with 10 neurons, one hidden layer with 20 neurons and finally, one output layer with only one neuron representing the output classes (normal and abnormal). Moreover, the values assumed for the ANN parameters are learning rate (0.001), momentum value (1.0000e⁻⁰³), number of training iterations (1000) and root mean square error <0.01. The foremost intention of the adaptive ANN is to classify the input US kidney images to normal/abnormal separation. To training the ANN structure, feed-forward back-propagation algorithm is utilized in our recommended procedure.

4.2.4.1 Adaptive Neural Networks Function Steps

The functioning steps involved in the proposed adaptive ANN are the following:

- Initialize weights randomly for every neurons except the neurons in the input layer.
- Optimize weights by OGSA.
- Develop the neural network with the selected image features, P_n (i.e. reduced feature) as the input units, Q_m as the hidden units and N/Ab as the output unit.

4.2.4.2 Opposition-based Gravitational Search Algorithm

The gravitational search algorithm (GSA) is stimulated by the laws of gravity and motion. The algorithm is gathered under a population-based method consisting of different masses. The masses share information to direct the search toward the best location in the search space based on the gravitational force. In the GSA, each mass (agent) encompasses four specifications: position, inertial mass, active gravitational mass and passive gravitational mass. The position of the mass signifies a solution of the issue, and its gravitational and inertial masses are decided by a fitness function. Therefore, each mass offers a solution, and the technique is directed by properly adapting the gravitational and inertia masses. The masses get attracted by the heaviest mass which intensely brings an optimum solution in the search space.

The steps involved in the OGSA algorithm are the following:

- Step 1: In terms of weights of ANN, population is initialized (i.e. $W = (w_1, w_2, \dots, w_n)$) within an interval [u, v]
- Step 2: Generate the opposite population of the weights initialized in Step 1. The oppositional solution is given as $W^* = u + v - W$
- Step 3: For populations generated in Steps 1 and 2, compute the fitness function (min MSE). The population that gives lesser fitness function value is chosen as the new initial population
- Step 4: The values of inertial masses and best and worst fitness function values are determined
- Step 5: The positions and velocities of the weights are updated
- Step 6: Repeat Steps 3-5 until the stopping criterion, i.e. maximum number of iterations, is reached

5 Results and Discussion

The proposed algorithm is executed using MATLAB software, and the experiment was carried out using a system with 4 GB of RAM and 2.10 GHz Intel i-3 processor.

For analysis, the US medical records of the patients with kidney problems as well as the US images of healthy persons were collected from various medical laboratories, particularly from the under pathology laboratories of Apollo Diagnostics and DDRC SRL Diagnostics Pvt Ltd in Tamil Nadu. The subject of data collections are men and women, with age ranging from 23 to 35 years. All subjects were encouraged to drink a lot of water 30 min before data collection to produce a clearer US image. Here, 26 abnormal and six normal US images were taken for the proposed classification method. The acquired data were preprocessed, analyzed and classified for detection of kidney disease in patients.

The experimental results for the diagnosis of kidney abnormality using the proposed OGSA-ANN approach and other similar machine-learning algorithms such as GSA-NN, ANN, GA-ANN, KNN and naive Bayes algorithms are analyzed in this section. The prediction efficiency is measured based on various factors.

5.1 Database Images

A few of the database images (normal and abnormal US kidney images) are shown in Figure 3.

5.2 Evaluation Metrics

The assessment metrics are sensitivity, specificity, false positive rate (FPR), false negative rate (FNR) and accuracy. The standard count values such as true positive (TP), true negative (TN), false positive (FP) and false negative (FN) are exploited here.

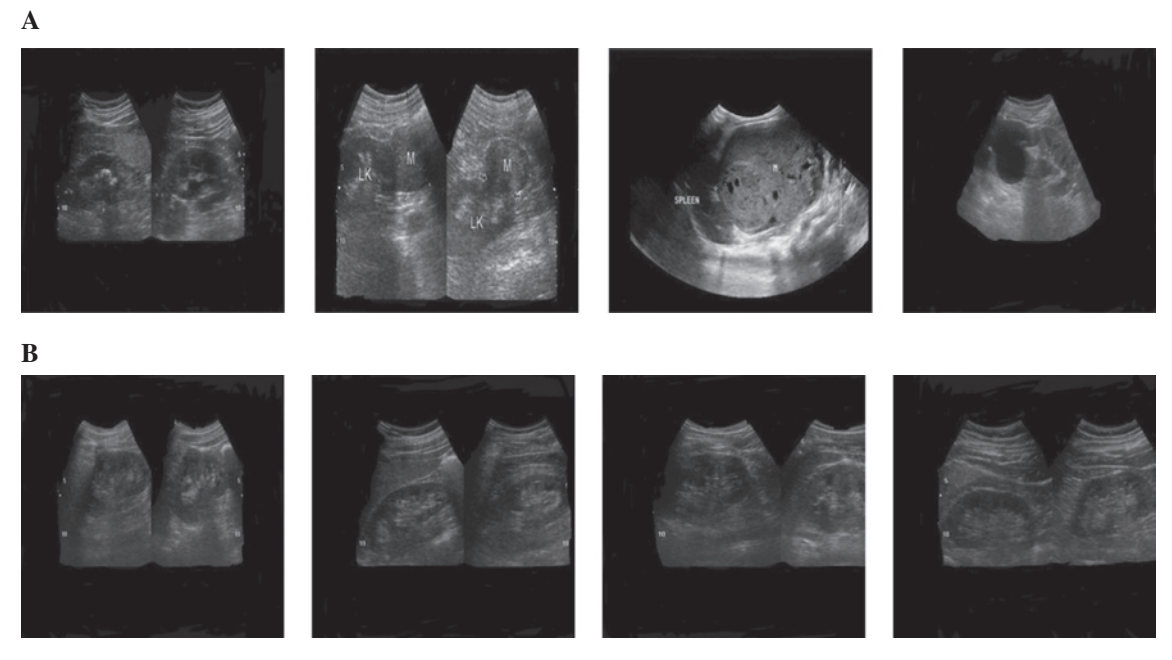


Figure 3: Some of the database images. Normal (A) and Abnormal (B) US Kidney Images.

Sensitivity =
$$\frac{\text{No. of TP}}{\text{No. of TP + No. of FN}} \times 100.$$
 (18)

Specificity: This is defined as the ratio of a number of TNs to the sum of TNs and FPs.

Specificity =
$$\frac{\text{No. of TN}}{\text{No. of TN + No. of FP}} \times 100.$$
 (19)

Accuracy: This can be calculated using the measures of sensitivity and specificity. It is denoted as

$$Accuracy = \frac{TP + TN}{TP + TN + FP + FN} \times 100.$$
 (20)

False-positive rate: The FPR, also known as the false-acceptance rate (FAR), refers to the proportion that all negative outcomes that yield positive test outcomes.

$$FPR = \frac{FP}{FP + TN} \times 100. \tag{21}$$

False-negative rate: The FNR, also known as the false-rejection rate (FRR), is the proportion of positive outcomes that yield negative test outcomes.

$$FNR = \frac{FN}{TP + FN} \times 100. \tag{22}$$

5.3 Performance Analysis

The performance assessment of the proposed adaptive ANN normal/abnormal kidney image classification method is shown in this section with various existing methods. The analysis is made on the basis of allowing 50% of samples for the training procedure and the remaining 50% samples for the testing process. The TP, TN, FP and FN values attained for the proposed and existing methods are given in Table 1.

Table 1 shows the FP and FN are low for the proposed OGSA-ANN approach compared with other approaches. However, there is no FP for naive Bayes, but the approach lacks in the prediction of normal images. The sensitivity, specificity and accuracy values computed from the above confusion matrix values are given in Table 2.

Table 2 shows that the specificity value is 100% for techniques like OGSA-ANN, KNN and naive Bayes algorithms, thus showing the better classification effectiveness of the proposed method. However, the GSA-based ANN, GA-based ANN and ANN techniques are offer <75%.

In the case of sensitivity, the proposed OGSA-ANN is 67%, which is better than the remaining techniques, whereas the ANN, KNN and naive Bayes algorithms offer null sensitivity, and 33% sensitivity is attained for the GSA- and GA-based ANN method.

Table 1: Confusion Matrix Values of Proposed and Existing Methods.

	OGSA-ANN	GSA-NN	ANN	GA-ANN	KNN	Naive Bayes
TP	2	1	0	1	0	0
TN	13	9	9	8	13	13
FP	0	4	4	5	0	0
FN	1	2	3	2	3	3

Table 2: Sensitivity, Specificity and Accuracy Values of Proposed and Existing Methods.

	OGSA-ANN	GSA-NN	ANN	GA-ANN	KNN	Naive Bayes
Sensitivity	0.666667	0.333333	0	0.333333	0	0
Specificity	1	0.692308	0.692308	0.615385	1	1
Accuracy	0.9375	0.625	0.5625	0.5625	0.8125	0.8125

Table 3: FAR, FRR and Accuracy Values of Proposed and Existing State-of-the-Art Methods.

Metrics	KNN [1] (%)	ARCK [2] (%)	MBPN [2] (%)	PNN [10] (%)	Proposed OGSA-ANN (%)
FAR	28.78	27.18	32.23	34.19	0
FRR	16.28	24.46	13.33	22.88	33.33
Accuracy	75.48	77.48	51	64.16	93.75

In Table 3, the result obtained for the proposed OGSA-ANN is in bold. While analyzing classification accuracy values, the proposed OGSA-based ANN provides 93%, whereas GSA-ANN gives 67%, GA-ANN and ANN give 53% and KNN and naive Bayes give 80%. Thus, the performance outcomes of the proposed strategy is markedly better in terms of accuracy, sensitivity and specificity measures and outperforms all the existing methods.

5.4 Performance Analysis with State-of-the-Art Methods

The FAR, FRR and accuracy values are compared and given in Table 3.

From the outcomes, the proposed approach clearly outperforms all other existing methods from Akkasaligar and Biradar [1], Dhanalakshmi and Rajamani [2] and Mangayarkarasi and Jamal [10]. The association rules with high confidence for kidney images (ARCK) method also gives 77% accuracy, whereas the proposed method gives 93%. Moreover, the FAR and FRR are also better for the proposed method compared with the existing methods.

6 Conclusion

An efficient abnormality classification method based on adaptive ANN is introduced to classify US kidney images. The classification efficiency is measured in terms of accuracy, sensitivity and specificity measures for the proposed as well as the existing methods like GSA-NN, ANN, GA-ANN, KNN, naive Bayes algorithms and other state-of-the-art methods. From the performance outcomes, the proposed adaptive ANN (i.e. OGSA-based ANN) achieves 94% classification accuracy, whereas the existing methods offer only less than the proposed one. Also, FAR is 0%, whereas the existing methods obtained FAR values not <27%. Thus, from the results obtained, it is clear that the proposed adaptive ANN works better in the classification of US kidney images than all the existing methods. In the future, multi-label classifications will be considered rather than normal/ abnormal characterization to examine the discriminative power of our approach for each sort of pathology.

Bibliography

[1] P. T. Akkasaligar and S. Biradar, Classification of medical ultrasound images of kidney, in: IJCA Proceedings on International Conference on Information and Communication Technologies (ICICT), Thrikkakara, Kerala, Vol. 3, 2014.

- [2] K. Dhanalakshmi and V. Rajamani, An efficient association rule-based method for diagnosing ultrasound kidney images, in: Computational Intelligence and Computing Research (ICCIC), 2010 IEEE International Conference on IEEE, Tamilnadu College of Engineering, Coimbatore, 2010.
- [3] T. Di Noia, V. Claudio Ostuni, F. Pesce, G. Binetti, D. Naso, F. Schena and E. Di Sciascio, An end stage kidney disease predictor based on an artificial neural networks ensemble, Exp. Syst. Appl. 40 (2013), 4438-4445.
- [4] A. Eklund, P. Dufort, D. Forsberg and S. M. La Conte, Medical image processing on the GPU past, present and future, Med. Image Anal. 17 (2013), 1073-1094.
- [5] S. Gunasundari, S. Janakiraman and S. Meenambal, Velocity bounded Boolean particle swarm optimization for improved feature selection in liver and kidney disease diagnosis, Exp. Syst. Appl. 56 (2016), 28-47.
- [6] A. Gupta and Karmeshu, Efficacy of Pearson distributions for characterization of gray levels in clinical ultrasound kidney images, Signal Image Video Process. 9 (2013), 1317-1334.
- [7] C. S. Gur and M. Top, Regional clustering of medical imaging technologies, Comput. Hum. Behav. 61 (2016), 333-343.
- [8] M.-K. Hu, Visual pattern recognition by moment invariants. IRE T. Inform. Theor. 8.2 (1962), 179-187.
- [9] J. Huang, X. Yang, Y. Chen and L. Tang, Ultrasound kidney segmentation with a global prior shape, J. Vis. Commun. Image Represent. 24 (2013), 937-943.
- [10] T. Mangayarkarasi and D. N. Jamal, PNN-based analysis system to classify renal pathologies in kidney ultrasound images, in: Computing and Communications Technologies (ICCCT), 2017 2nd International Conference on IEEE, Chennai, 2017.
- [11] R. Odeh, D. Noone, P. Bowlin, L. H. P. Braga and A. J. Lorenzo, Predicting risk of chronic kidney disease in infants and young children at diagnosis of posterior urethral valves: initial ultrasound kidney characteristics and validation of parenchymal area as forecasters of renal reserve, J. Urol. 196 (2016), 862-868.
- [12] O. Reiche, K. Häublein, M. Reichenbach, M. Schmid, F. Hannig, J. Teich and D. Fey, Synthesis and optimization of image processing accelerators using domain knowledge, J. Syst. Architect. 61 (2015), 646-658.
- [13] F. Rengier, M. F. Häfnerb, R. Unterhinninghofenc, R. Nawrotzkid, J. Kirsch, H.-U. Kauczor and F. L. Giesel, Integration of interactive three-dimensional image post-processing software into undergraduate radiology education effectively improves diagnostic skills and visual-spatial ability, Eur. J. Radiol. 82 (2013), 1366-1371.
- [14] L. Sajn and M. Kukar, Image processing and machine learning for fully automated probabilistic evaluation of medical images, Comput. Methods Prog. Biomed. 104 (2011), e75-e86.
- [15] M. B. Subramanya, V. Kumar, S. Mukherjee and M. Saini, SVM-based CAC system for B-mode kidney ultrasound images, J. Dig. Imaging 28 (2014), 448-458.
- [16] A. Świetlicka, Trained stochastic model of biological neural network used in image processing task, Appl. Math. Comput. 267 (2015), 716-726.
- [17] J. Tian, J. Xue, Y. Dai, J. Chen and J. Zheng, A novel software platform for medical image processing and analyzing, IEEE Trans. Inf. Technol. Biomed. 12 (2008), 800-812.
- [18] M. E. Tipping and C. M. Bishop, Probabilistic principal component analysis, J. R. Stat. Soc. B Stat. Method. 61 (1999), 611-622
- [19] F. Zhao, J. Zhao, W. Zhao, F. Qu and L. Sui, Local region statistics combining multi-parameter intensity fitting module for medical image segmentation with intensity in homogeneity and complex composition, Optics Laser Technol. 82 (2016),